ACS Catalysis

Research Article

Cite This: ACS Catal. 2018, 8, 10131−10136

pubs.acs.org/acscatalysis

Unusual Stability of a Bacteriochlorin Electrocatalyst under Reductive Conditions. A Case Study on CO_2 Conversion to CO

Jianbing Jiang,[†,‡] Adam J. Matula,[†,‡] John R. Swierk,[†,‡] Neyen Romano,[†,‡] Yueshen Wu,[†,‡] Victor S. Batista,[*,†,‡] Robert H. Crabtree,[*,†,‡] Jonathan S. Lindsey,[*,§] Hailiang Wang,[*,†,‡] and Gary W. Brudvig[*,†,‡]

[†]Department of Chemistry, Yale University, New Haven, Connecticut 06520, United States

[‡]Energy Sciences Institute, Yale University, West Haven, Connecticut 06516, United States

[§]Department of Chemistry, North Carolina State University, Raleigh, North Carolina 27695, United States

Supporting Information

ABSTRACT: Photosynthetic CO_2 fixation is mediated by the enzyme RuBisCo, which employs a nonredox-active metal (Mg^{2+}) to bind CO_2 adjacent to an organic ligand that provides reducing equivalents for CO_2 fixation. Attempts to use porphyrins as ligands in reductive catalysis have typically encountered severe stability issues owing to ligand reduction. Here, a synthetic zinc−bacteriochlorin is reported as an effective and robust electrocatalyst for CO_2 reduction to CO with an overpotential of 330 mV, without undergoing porphyrin-like ligand degradation (or demetalation) even after prolonged bulk electrolysis. The reaction has a CO Faradaic efficiency of 92% and sustains a total current density of 2.3 mA/cm^2 at −1.9 V vs Ag/AgCl. DFT calculations highlight the molecular origin of the observed stability and provide insights into catalytic steps. This bioinspired study opens avenues for the application of bacteriochlorin compounds for reductive electrocatalysis with extended life beyond that seen with porphyrin counterparts.

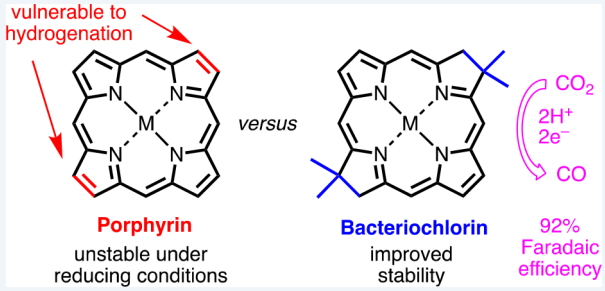

KEYWORDS: *bacteriochlorin, CO_2 conversion, electrocatalysis, hydrogenation, porphyrin*

INTRODUCTION

The photosynthetic fixation of carbon, a global process of immense ecological importance, is catalyzed by the enzyme RuBisCo. While an elaborate protein architecture, the enzyme-mediated reduction relies on a nonredox-active metal (Mg(II)) and an organic ligand that provides reducing equivalents. Efforts toward abiological carbon fixation typically have turned to use redox-active metals.[1−6] Metalloporphyrins have been widely used as tetradentate ligands in photo- and electrocatalysis[1,2,7−10] and are particularly attractive in part given the availability of mature synthetic routes to access structurally sophisticated architectures.[11−14] However, though some porphyrin systems are stable enough under mild electrochemical conditions,[15] a long-standing problem of porphyrin ligands—regardless of the nature or presence of the metal—is their instability under reductive and protic conditions, forming chlorins (C,C′-dihydroporphyrins), phlorins (C,N-dihydroporphyrins), isobacteriochlorins (tetrahydroporphyrins), or a mixture thereof by hydrogenation of one or both of the double bonds in the porphyrin 2*H*-pyrrole rings (Chart 1A).[16−20] Such undesired transformation leads to low Faradaic efficiency of electrocatalysis because some of the reducing equivalents are supplied to drive the $2e^-/2H^+$ or $4e^-/4H^+$ hydrogenation reactions.[19−21] In addition, the resulting chlorin and phlorin catalysts have different light-harvesting properties and charge-separated states when compared to their precursors,[22,23] which complicates the photocatalytic processes.[19,20,24−26] For example, our previous work with Sb−porphyrin complexes has shown efficient hydrogen evolution but also irreversible porphyrin ligand reduction and thus low Faradaic efficiency.[20] In a series of rhenium−porphyrin dyads for CO_2 photoreduction, Windle et al. found that photoabsorption by the porphyrin induced 2-electron hydrogenation to form a chlorin first followed by another 2-electron hydrogenation to form an isobacteriochlorin, ultimately completely altering the Q-band region of the porphyrin spectrum.[19] Such instability currently hinders the greater practical utility of porphyrins in applications to reductive electrocatalysis.

Bacteriochlorins are the core chromophores of natural bacteriochlorophylls that are already reduced so they are not vulnerable to hydrogenation reactions of a 2*H*-pyrrole ring as in porphyrins. In addition, synthetic bacteriochlorins[27−30] that are equipped with a geminal dimethyl group in each reduced (pyrroline) unit have been shown to be stable toward adventitious dehydrogenation (Chart 1B). These bacterio-

Received: July 28, 2018
Revised: September 14, 2018
Published: September 20, 2018

DOI: 10.1021/acscatal.8b02991
ACS Catal. 2018, 8, 10131−10136

Chart 1. (A) Structure of a Porphyrin Framework. (B) Molecular Design of a Synthetic Bacteriochlorin. (C) Chemical Structure of the Synthetic Bacteriochlorin (ZnBC) Introduced in This Work

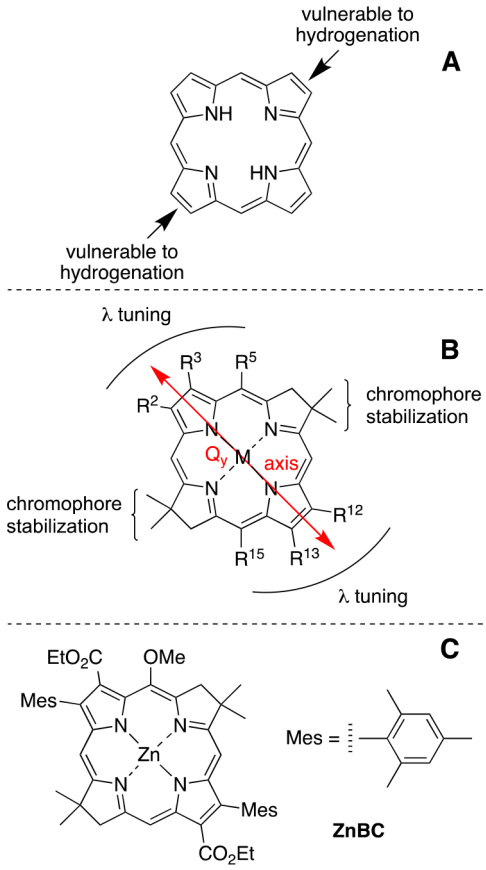

chlorins exhibit superior stability versus porphyrins, and their absorption spectrum can be easily tuned throughout the UV, visible, and near-infrared (NIR) regions by suitable modifications with substituents along the Q_y axis.[28] Bacteriochlorins have already been used as chromophores for light-harvesting,[31−33] as photosensitizers for photodynamic therapy,[34,35] and as fluorophores for clinical diagnostics and cell imaging,[30,36] but up to now have not been explored as ligands in electrochemistry and catalysis.

Here, we report the synthesis and characterization of a gem-dimethyl-substituted zinc(II) bacteriochlorin. As proof-of-concept, the zinc−bacteriochlorin complex was found to be a stable and efficient electrocatalyst for CO_2-to-CO conversion as shown by the rather high (92%) Faradaic efficiency. To the best of our knowledge, this is the first demonstration of a bacteriochlorin ligand for efficient electrocatalysis. The work was inspired by consideration of core conceptual features of the RuBisCo enzyme. We anticipate this bioinspired study may open new avenues for the application of zinc−bacteriochlorins (and other redox-inert metal−ligand complexes) for studies requiring extended reductive electrocatalytic duration, particularly where the porphyrin counterparts have proved susceptible to reductive degradation.

RESULTS AND DISCUSSION

The zinc−bacteriochlorin **ZnBC** (Chart 1C) was prepared by following a reported procedure[37] and was characterized by ICP-MS (Table S1) to confirm the complete removal of free zinc or other possible metal salts (NaCl, etc.) that could otherwise interfere in the catalytic process. The electrochemical properties of **ZnBC** were studied by cyclic voltammetry (CV) using glassy carbon as the working electrode in DMF with 5 M water and 0.5 mM of **ZnBC** and 0.1 M tetrabutylammonium hexafluorophosphate as the supporting electrolyte.

Under reducing conditions, the cyclic voltammogram of **ZnBC** shows two reversible peaks at −0.95 and −1.37 V vs Ag/AgCl (Figure 1), corresponding to the radical anion and

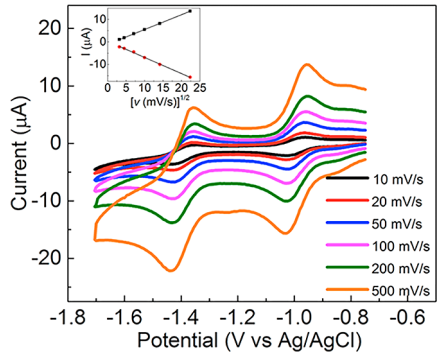

Figure 1. Scan-rate-dependent CV of 0.5 mM **ZnBC** in DMF with 5 M H_2O. Inset: square root of scan rate versus current for the first reduction peak.

dianion, respectively. The plots of peak current versus square root of the scan rate are linear (Figure 1 inset), indicative of diffusion-controlled processes.

Reduction potentials calculated by density functional theory (DFT)[38] are in broad agreement with the experimental results, yielding calculated potentials of −1.03 and −1.65 V vs Ag/AgCl. Notably, calculations show that the reducing equivalents are delocalized on the bacteriochlorin ring, with negligible changes of electron density on the metallic center. The resulting electron density has essentially the same distribution as in the LUMO of the parent species (Figure S1A). Therefore, the calculations suggest that **ZnBC** has a redox-active ligand and a redox-innocent metal center, akin to zinc porphyrin systems from our group.[9] Redox noninnocence of ligands has attracted much attention in catalysis, and the resulting changes in electron distribution suggest mechanistic implications.[39] Notably, the geometry of **ZnBC** changes very little upon reduction, showing just a slight puckering of the ring with an N−N−N−N dihedral angle increase from a nearly planar 1° in the nonreduced case to 3° and 4° in the singly and doubly reduced cases, respectively (Figure S1B).

Catalytic CO_2 electroreduction was first seen by comparing CV measurements under an argon or CO_2 atmosphere, using DMF containing water (5 M) as the proton source (Figure 2A). In an argon atmosphere, significant current was observed after −1.8 V vs Ag/AgCl, attributed to proton reduction at this highly negative potential (red trace in Figure 2A). In a CO_2 atmosphere, a cathodic current increase was observed at the less negative potential of −1.5 V vs Ag/AgCl (blue trace in Figure 2A), corresponding to CO_2 reduction with an overpotential of 330 mV (the corrected thermodynamic potential in DMF/H_2O (5 M) is 1.17 V, see the Supporting Information for details).

Controlled-potential electrolysis (CPE) of **ZnBC** at various potentials was performed for electrochemical CO_2 reduction in

DOI: 10.1021/acscatal.8b02991
ACS Catal. 2018, 8, 10131−10136

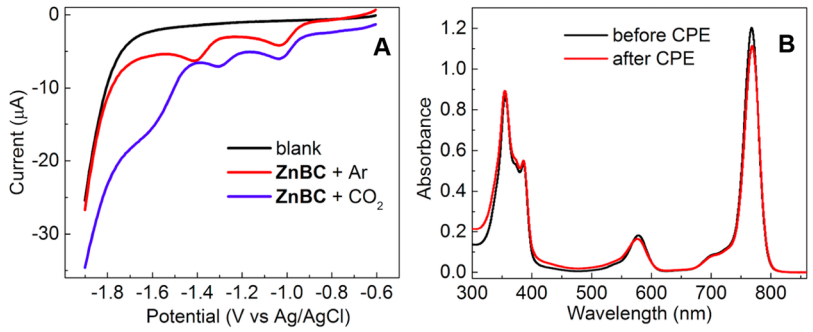

Figure 2. (A) CV scans of electrolyte solution without catalyst **ZnBC** (black), with **ZnBC** under an argon atmosphere (red), and with **ZnBC** under a CO_2 atmosphere (blue). Only cathodic traces are displayed for clarity. (B) Absorption spectra of the electrolyte solution before (black) and after (red) 4 h of CPE. The same amounts of aliquots from the electrolyte solution were used.

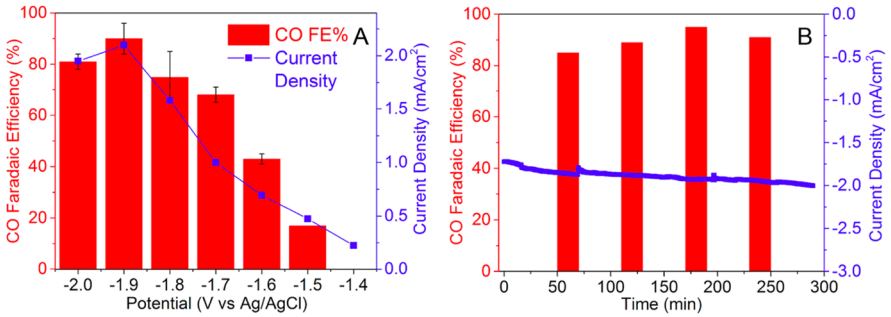

Figure 3. (A) CO Faradaic efficiencies and total current densities at various potentials (averaged from two measurements). (B) CO Faradaic efficiencies and total current densities after 1, 2, 3, and 4 h of electrolysis at −1.9 V vs Ag/AgCl. H_2 gas is the only other reduction product in all measurements.

DMF with 5 M water, using high-surface-area carbon fiber paper as the working electrode. ^{1}H NMR spectroscopy and gas chromatography allowed detection of liquid and gaseous products. At all selected potentials, no liquid product was detected (Figure S2). Only CO and H_2 were detected as the gaseous products. The CO Faradaic efficiency and total current density at various potentials are shown in Figure 3A. With more negative potentials applied to the catalyst electrode, higher CO Faradaic efficiencies and total current densities were observed. The highest CO Faradaic efficiency of 92% and total current density of 2.3 mA/cm^2 were achieved at −1.9 V vs Ag/AgCl. This potential (−1.9 V vs Ag/AgCl) was selected for CPE. High CO Faradaic efficiency (92%) and total current density (2.3 mA/cm^2) were held for over 4 h (Figure 3B), indicating excellent stability of the catalyst **ZnBC**. CPE using zinc-free bacteriochlorin under the same electrocatalytic conditions did not afford any detectable CO_2 reduction product, suggesting the role of the zinc center as a binding site for CO_2.

To confirm that the molecular integrity of **ZnBC** is retained and that no bacteriochlorin ligand degradation or demetalation occurred during bulk electrolysis, the UV−vis−NIR spectra of the electrolyte solution were recorded before and after the bulk electrolysis (Figure 2B). The two spectra are nearly identical, indicating no ligand degradation or demetalation during CPE. Transmission electron microscopy (TEM), energy dispersive X-ray spectroscopy (EDS), and X-ray photoelectron spectroscopy (XPS) were also performed on the carbon fiber paper after CPE (Figure S3). The absence of the zinc signal in the EDS and XPS spectra ruled out the possibility of zinc demetalation at the carbon electrode. The carbon electrode was gently washed with DMF after a 4-h electrolysis and again used as the working electrode in a fresh electrolyte solution without **ZnBC**. No CO_2 reduction was observed, further confirming that the active species for CO_2 reduction is **ZnBC** under homogeneous conditions rather than deposited **ZnBC** or zinc metal on the carbon electrode.

Potential binding modes of CO_2 on **ZnBC** were examined via DFT calculations (Figure 4). Comparing the minimum energy binding configurations of CO_2 on **ZnBC** in its nonreduced form as well as after the first and second reduction indicates that significant activation of the C−O bond occurs only after the second reduction. Without two reductions, CO_2 remains unreactive. However, upon the second reduction, CO_2 is reduced in agreement with the open circuit absorption spectrum and CV results. A full mechanistic analysis is outside the scope of this paper and will be reported elsewhere including additional experimental and computational results,[40] consistent with CO_2 binding to the doubly reduced **ZnBC** complex.

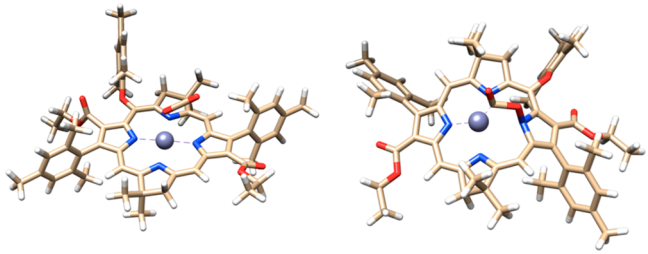

Figure 4. Calculated minimum energy structure of CO_2 on nonreduced (left) **ZnBC** and doubly reduced (right) **ZnBC**.

DOI: 10.1021/acscatal.8b02991
ACS Catal. 2018, 8, 10131−10136

To further probe the stability of the bacteriochlorin ligand, absorption spectroscopy was used to monitor the changes of free-base bacteriochlorin **BC** and porphyrin **Porph** (Chart 2).

Chart 2. Bacteriochlorin BC and Porphyrin Porph for Stability Comparison

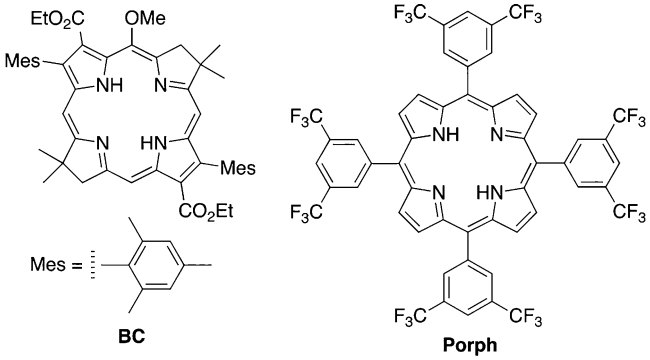

The fluorinated porphyrin **Porph** was selected for comparison because of the following: (1) the first two reduction potentials of **Porph** are close (within 0.2 V difference) to those of **BC**, which helps minimize effects arising from the different redox properties of the bacteriochlorin and porphyrin; and (2) **Porph** has sufficient solubility in DMF with 5 M H_2O, while many other porphyrins are poorly soluble (0.5 mM) in the same mixed solvent. During the stability test at −1.9 V vs Ag/AgCl, aliquots of the solution were taken out of the electrolysis cell and exposed to air for 5 min before absorption measurement. The shape and intensity of the absorption spectra of **BC** remained almost unchanged over the first 4 h. A 30% loss of spectral intensity was observed (albeit without a concurrent change in spectral shape) after an additional 20 h, indicating some degradation occurred during 20 h of electrolysis. In comparison, the absorption spectra of **Porph** underwent a dramatic change; the Soret band intensity decreased by 60% within the first 3 h, with a shape change and intensity increase in the Q-band region (Figure S4). The two new bands at 650 and 730 nm were attributed to the generation of two porphyrin hydrogenation products, phlorin and isobacteriochlorin.[16,19] Prolonged electrolysis (a total of 22 h) led to complete bleaching of the porphyrin bands, indicating total degradation of the porphyrin under the reducing conditions. High-resolution ESI-MS was performed on the samples at different time points to detect the hydrogenated species, but no phlorin or isobacteriochlorin peak was detected, probably due to the short lifetimes of these two species. The comparison of bacteriochlorin **BC** and a representative porphyrin clearly shows that the bacteriochlorin framework affords superior stability over a porphyrin structure.

To probe the molecular underpinnings of this stability difference as well as other potential differences between the porphyrin and bacteriochlorin frameworks, a computational case study was made of two simplified structures (Figure S5A). These structures were chosen because they offer an opportunity to explore the differences in the two frameworks alone, and their simplified structures make visualization correspondingly simpler. In porphyrins, many relevant chemical properties, including absorption spectroscopy, are related to the four Gouterman orbitals.[41] Comparing these orbitals (HOMO−1, HOMO, LUMO, and LUMO+1) in the two structures (Figure S5B) shows key differences that can be directly linked to their stability. At this level, the primary differences between the two species are related to their orbital symmetries and their corresponding energetics (Figure S6). In porphyrins, the HOMO and HOMO−1 as well as the LUMO and LUMO+1 are nearly degenerate, and this system is no exception. In the bacteriochlorin species, however, the additional reduction has the effect of interfering with the orbital symmetry at these sites, breaking this degeneracy. Frontier molecular orbital (FMO) theory suggests that reactivity is largely determined by the frontier orbitals, and for a hydrogenation reaction the relevant orbital is the molecular LUMO, which is populated upon reduction. Close examination of these LUMOs shows that in porphyrins, there is significant electron density at the double bonds vulnerable to hydrogenation, while in the case of bacteriochlorin the corresponding bonds (and the carbon atoms they encompass) have no significant electron density, precluding reactivity. The case study presented here uses zinc-metalated porphyrin and bacteriochlorin frameworks, but the same results are seen without zinc (Figures S7 and S8).

CONCLUSIONS

In conclusion, we have studied the electrochemical properties of a novel zinc(II)−bacteriochlorin complex under severe reducing conditions. A comparison between the bacteriochlorin ligand and a porphyrin analogue confirmed the superior stability of the bacteriochlorin. Application of the zinc−bacteriochlorin complex to electrocatalytic CO_2-to-CO conversion resulted in high Faradaic efficiency (92%) and excellent catalyst stability. No ligand decomposition or zinc demetalation occurred during prolonged bulk electrolysis, indicating a truly molecular catalytic species. Computational results compared favorably with experimental voltammogram evidence suggesting that CO_2 binding is induced upon double reduction of **ZnBC**. To the best of our knowledge, this is the first study of a bacteriochlorin ligand for efficient electrocatalysis. Our findings suggest the viability of employing bacteriochlorin-based catalysts for various catalytic processes, even under strongly reducing conditions. Finally, we note that the present approach is bioinspired in two respects. First, the enzyme for photosynthetic carbon fixation, RuBisCo, relies on nonredox-active Mg(II) and an organic ligand that provides reducing equivalents. Second, the strategy of using gem-dialkyl groups to secure the stability of a tetrapyrrole macrocycle mirrors the natural electrocatalytic macrocycles, cobalamin and F_{430},[42] which are pervasively substituted with gem-dialkyl groups in the reduced rings.

ASSOCIATED CONTENT

Supporting Information

The Supporting Information is available free of charge on the ACS Publications website at DOI: 10.1021/acscatal.8b02991.

Instruments, experimental details, additional figures, and additional computation and characterization data (PDF)

AUTHOR INFORMATION

Corresponding Authors

*E-mail: victor.batista@yale.edu.
*E-mail: robert.crabtree@yale.edu.
*E-mail: jlindsey@ncsu.edu.
*E-mail: hailiang.wang@yale.edu.
*E-mail: gary.brudvig@yale.edu.

DOI: 10.1021/acscatal.8b02991
ACS Catal. 2018, 8, 10131−10136

ORCID

John R. Swierk: 0000-0001-5811-7285
Victor S. Batista: 0000-0002-3262-1237
Robert H. Crabtree: 0000-0002-6639-8707
Jonathan S. Lindsey: 0000-0002-4872-2040
Hailiang Wang: 0000-0003-4409-2034
Gary W. Brudvig: 0000-0002-7040-1892

Notes

The authors declare no competing financial interest.

■ ACKNOWLEDGMENTS

This work was supported by the U.S. Department of Energy, Chemical Sciences, Geosciences, and Biosciences Division, Office of Basic Energy Sciences, Office of Science (DE-FG02-07ER15909, DE-FG02-05ER15661). The electrocatalytic work was partially supported by the National Science Foundation (Grant CHE-1651717). Additional support was provided by a generous gift from the TomKat Foundation. We thank the Yale West Campus Analytical Core and Yale West Campus Materials Characterization Core for help with NMR and electron microscopy measurements. Computational resources were provided by NERSC and the Yale Center for Research Computing. A.J.M. was supported by the National Science Foundation Graduate Research Fellowship under Grant No. DGE-1122492.

■ REFERENCES

(1) Costentin, C.; Drouet, S.; Robert, M.; Saveant, J. M. A Local Proton Source Enhances CO_2 Electroreduction to CO by a Molecular Fe Catalyst. *Science* **2012**, *338*, 90−94.
(2) Costentin, C.; Robert, M.; Saveant, J. M.; Tatin, A. Efficient and Selective Molecular Catalyst for the CO_2-to-CO Electrochemical Conversion in Water. *Proc. Natl. Acad. Sci. U. S. A.* **2015**, *112*, 6882−6886.
(3) Costentin, C.; Drouet, S.; Robert, M.; Saveant, J. M. Turnover Numbers, Turnover Frequencies, and Overpotential in Molecular Catalysis of Electrochemical Reactions. Cyclic Voltammetry and Preparative-Scale Electrolysis. *J. Am. Chem. Soc.* **2012**, *134*, 11235−11242.
(4) Shen, J.; Kortlever, R.; Kas, R.; Birdja, Y. Y.; Diaz-Morales, O.; Kwon, Y.; Ledezma-Yanez, I.; Schouten, K. J.; Mul, G.; Koper, M. T. Electrocatalytic Reduction of Carbon Dioxide to Carbon Monoxide and Methane at an Immobilized Cobalt Protoporphyrin. *Nat. Commun.* **2015**, *6*, 8177.
(5) Hod, I.; Sampson, M. D.; Deria, P.; Kubiak, C. P.; Farha, O. K.; Hupp, J. T. Fe-Porphyrin-Based Metal−Organic Framework Films as High-Surface Concentration, Heterogeneous Catalysts for Electrochemical Reduction of CO_2. *ACS Catal.* **2015**, *5*, 6302−6309.
(6) Liu, C.; Colon, B. C.; Ziesack, M.; Silver, P. A.; Nocera, D. G. Water Splitting-Biosynthetic System with CO_2 Reduction Efficiencies Exceeding Photosynthesis. *Science* **2016**, *352*, 1210−1213.
(7) Weng, Z.; Jiang, J.; Wu, Y.; Wu, Z.; Guo, X.; Materna, K. L.; Liu, W.; Batista, V. S.; Brudvig, G. W.; Wang, H. Electrochemical CO_2 Reduction to Hydrocarbons on a Heterogeneous Molecular Cu Catalyst in Aqueous Solution. *J. Am. Chem. Soc.* **2016**, *138*, 8076−8079.
(8) Hu, X. M.; Ronne, M. H.; Pedersen, S. U.; Skrydstrup, T.; Daasbjerg, K. Enhanced Catalytic Activity of Cobalt Porphyrin in CO_2 Electroreduction Upon Immobilization on Carbon Materials. *Angew. Chem., Int. Ed.* **2017**, *56*, 6468−6472.
(9) Wu, Y.; Jiang, J.; Weng, Z.; Wang, M.; Broere, D. L. J.; Zhong, Y.; Brudvig, G. W.; Feng, Z.; Wang, H. Electroreduction of CO_2 Catalyzed by a Heterogenized Zn-Porphyrin Complex with a Redox-Innocent Metal Center. *ACS Cent. Sci.* **2017**, *3*, 847−852.
(10) Zhang, H.; Wei, J.; Dong, J.; Liu, G.; Shi, L.; An, P.; Zhao, G.; Kong, J.; Wang, X.; Meng, X.; Zhang, J.; Ye, J. Efficient Visible-Light-Driven Carbon Dioxide Reduction by a Single-Atom Implanted Metal-Organic Framework. *Angew. Chem., Int. Ed.* **2016**, *55*, 14310−14314.
(11) Senge, M. O.; Shaker, Y. M.; Pintea, M.; Ryppa, C.; Hatscher, S. S.; Ryan, A.; Sergeeva, Y. Synthesis of meso-Substituted ABCD-Type Porphyrins by Functionalization Reactions. *Eur. J. Org. Chem.* **2010**, *2010*, 237−258.
(12) Lindsey, J. S. Synthetic Routes to meso-Patterned Porphyrins. *Acc. Chem. Res.* **2010**, *43*, 300−311.
(13) Senge, M. O. Stirring the Porphyrin Alphabet Soup − Functionalization Reactions for Porphyrins. *Chem. Commun.* **2011**, *47*, 1943−1960.
(14) Zhang, Z.; Gao, W. Y.; Wojtas, L.; Ma, S.; Eddaoudi, M.; Zaworotko, M. J. Post-Synthetic Modification of Porphyrin-Encapsulating Metal-Organic Materials by Cooperative Addition of Inorganic Salts to Enhance CO_2/CH_4 Selectivity. *Angew. Chem., Int. Ed.* **2012**, *51*, 9330−9334.
(15) Azcarate, I.; Costentin, C.; Robert, M.; Saveant, J. M. Through-Space Charge Interaction Substituent Effects in Molecular Catalysis Leading to the Design of the Most Efficient Catalyst of CO_2-to-CO Electrochemical Conversion. *J. Am. Chem. Soc.* **2016**, *138*, 16639−16644.
(16) Solis, B. H.; Maher, A. G.; Dogutan, D. K.; Nocera, D. G.; Hammes-Schiffer, S. Nickel Phlorin Intermediate Formed by Proton-Coupled Electron Transfer in Hydrogen Evolution Mechanism. *Proc. Natl. Acad. Sci. U. S. A.* **2016**, *113*, 485−492.
(17) Tamiaki, H.; Monobe, R.; Koizumi, S.; Miyatake, T.; Kinoshita, Y. Stereoselective Reduction, Methylation, and Phenylation of the 13-Carbonyl Group in Chlorophyll Derivatives. *Tetrahedron: Asymmetry* **2013**, *24*, 967−972.
(18) Bruhn, T.; Bruckner, C. Origin of the Regioselective Reduction of Chlorins. *J. Org. Chem.* **2015**, *80*, 4861−4868.
(19) Windle, C. D.; George, M. W.; Perutz, R. N.; Summers, P. A.; Sun, X. Z.; Whitwood, A. C. Comparison of Rhenium−Porphyrin Dyads for CO_2 Photoreduction: Photocatalytic Studies and Charge Separation Dynamics Studied by Time-Resolved IR Spectroscopy. *Chem. Sci.* **2015**, *6*, 6847−6864.
(20) Jiang, J.; Materna, K. L.; Hedström, S.; Yang, K. R.; Crabtree, R. H.; Batista, V. S.; Brudvig, G. W. Antimony Complexes for Electrocatalysis: Activity of a Main-Group Element in Proton Reduction. *Angew. Chem., Int. Ed.* **2017**, *56*, 9111−9115.
(21) Agarwal, J.; Fujita, E.; Schaefer, H. F., 3rd; Muckerman, J. T. Mechanisms for CO Production from CO_2 Using Reduced Rhenium Tricarbonyl Catalysts. *J. Am. Chem. Soc.* **2012**, *134*, 5180−5186.
(22) Lu, G.; Jiang, X.; Ou, Z.; Yan, S.; Kadish, K. M. Solvent and Substituent Effects on UV-Vis Spectra and Redox Properties of Zinc P-Hydroxylphenylporphyrins. *J. Porphyrins Phthalocyanines* **2017**, *21*, 465−475.
(23) Rybicka-Jasinska, K.; Shan, W.; Zawada, K.; Kadish, K. M.; Gryko, D. Porphyrins as Photoredox Catalysts: Experimental and Theoretical Studies. *J. Am. Chem. Soc.* **2016**, *138*, 15451−15458.
(24) Terazono, Y.; Kodis, G.; Chachisvilis, M.; Cherry, B. R.; Fournier, M.; Moore, A.; Moore, T. A.; Gust, D. Multiporphyrin Arrays with Pi-Pi Interchromophore Interactions. *J. Am. Chem. Soc.* **2015**, *137*, 245−258.
(25) Doherty, M. D.; Grills, D. C.; Muckerman, J. T.; Polyansky, D. E.; Fujita, E. Toward More Efficient Photochemical CO_2 Reduction: Use of $scCO_2$ or Photogenerated Hydrides. *Coord. Chem. Rev.* **2010**, *254*, 2472−2482.
(26) Vengris, M.; Larsen, D. S.; Valkunas, L.; Kodis, G.; Herrero, C.; Gust, D.; Moore, T.; Moore, A.; van Grondelle, R. Separating Annihilation and Excitation Energy Transfer Dynamics in Light Harvesting Systems. *J. Phys. Chem. B* **2013**, *117*, 11372−11382.
(27) Krayer, M.; Ptaszek, M.; Kim, H. J.; Meneely, K. R.; Fan, D.; Secor, K.; Lindsey, J. S. Expanded Scope of Synthetic Bacteriochlorins Via Improved Acid Catalysis Conditions and Diverse Dihydrodipyrrin-Acetals. *J. Org. Chem.* **2010**, *75*, 1016−1039.

DOI: 10.1021/acscatal.8b02991
ACS Catal. 2018, 8, 10131−10136

(28) Reddy, K. R.; Jiang, J.; Krayer, M.; Harris, M. A.; Springer, J. W.; Yang, E.; Jiao, J.; Niedzwiedzki, D. M.; Pandithavidana, D.; Parkes-Loach, P. S.; Kirmaier, C.; Loach, P. A.; Bocian, D. F.; Holten, D.; Lindsey, J. S. Palette of Lipophilic Bioconjugatable Bacteriochlorins for Construction of Biohybrid Light-Harvesting Architectures. *Chem. Sci.* **2013**, *4*, 2036−2053.
(29) Kim, H. J.; Lindsey, J. S. De Novo Synthesis of Stable Tetrahydroporphyrinic Macrocycles: Bacteriochlorins and a Tetradehydrocorrin. *J. Org. Chem.* **2005**, *70*, 5475−5486.
(30) Zhang, N.; Jiang, J.; Liu, M.; Taniguchi, M.; Mandal, A. K.; Evans-Storms, R. B.; Pitner, J. B.; Bocian, D. F.; Holten, D.; Lindsey, J. S. Bioconjugatable, Pegylated Hydroporphyrins for Photochemistry and Photomedicine. Narrow-Band, near-Infrared-Emitting Bacteriochlorins. *New J. Chem.* **2016**, *40*, 7750−7767.
(31) Jiang, J.; Reddy, K. R.; Pavan, M. P.; Lubian, E.; Harris, M. A.; Jiao, J.; Niedzwiedzki, D. M.; Kirmaier, C.; Parkes-Loach, P. S.; Loach, P. A.; Bocian, D. F.; Holten, D.; Lindsey, J. S. Amphiphilic, Hydrophilic, or Hydrophobic Synthetic Bacteriochlorins in Biohybrid Light-Harvesting Architectures: Consideration of Molecular Designs. *Photosynth. Res.* **2014**, *122*, 187−202.
(32) Jiang, J.; Taniguchi, M.; Lindsey, J. S. Near-Infrared Tunable Bacteriochlorins Equipped for Bioorthogonal Labeling. *New J. Chem.* **2015**, *39*, 4534−4550.
(33) Springer, J. W.; Parkes-Loach, P. S.; Reddy, K. R.; Krayer, M.; Jiao, J.; Lee, G. M.; Niedzwiedzki, D. M.; Harris, M. A.; Kirmaier, C.; Bocian, D. F.; Lindsey, J. S.; Holten, D.; Loach, P. A. Biohybrid Photosynthetic Antenna Complexes for Enhanced Light-Harvesting. *J. Am. Chem. Soc.* **2012**, *134*, 4589−4599.
(34) Huang, Y. Y.; Mroz, P.; Zhiyentayev, T.; Sharma, S. K.; Balasubramanian, T.; Ruzie, C.; Krayer, M.; Fan, D.; Borbas, K. E.; Yang, E.; Kee, H. L.; Kirmaier, C.; Diers, J. R.; Bocian, D. F.; Holten, D.; Lindsey, J. S.; Hamblin, M. R. In Vitro Photodynamic Therapy and Quantitative Structure-Activity Relationship Studies with Stable Synthetic near-Infrared-Absorbing Bacteriochlorin Photosensitizers. *J. Med. Chem.* **2010**, *53*, 4018−4027.
(35) Panchenko, P. A.; Grin, M. A.; Fedorova, O. A.; Zakharko, M. A.; Pritmov, D. A.; Mironov, A. F.; Arkhipova, A. N.; Fedorov, Y. V.; Jonusauskas, G.; Yakubovskaya, R. I.; Morozova, N. B.; Ignatova, A. A.; Feofanov, A. V. A Novel Bacteriochlorin-Styrylnaphthalimide Conjugate for Simultaneous Photodynamic Therapy and Fluorescence Imaging. *Phys. Chem. Chem. Phys.* **2017**, *19*, 30195−30206.
(36) Harada, T.; Sano, K.; Sato, K.; Watanabe, R.; Yu, Z.; Hanaoka, H.; Nakajima, T.; Choyke, P. L.; Ptaszek, M.; Kobayashi, H. Activatable Organic near-Infrared Fluorescent Probes Based on a Bacteriochlorin Platform: Synthesis and Multicolor in vivo Imaging with a Single Excitation. *Bioconjugate Chem.* **2014**, *25*, 362−369.
(37) Chen, C. Y.; Sun, E.; Fan, D.; Taniguchi, M.; McDowell, B. E.; Yang, E.; Diers, J. R.; Bocian, D. F.; Holten, D.; Lindsey, J. S. Synthesis and Physicochemical Properties of Metallobacteriochlorins. *Inorg. Chem.* **2012**, *51*, 9443−9464.
(38) Konezny, S. J.; Doherty, M. D.; Luca, O. R.; Crabtree, R. H.; Soloveichik, G. L.; Batista, V. S. Reduction of Systematic Uncertainty in DFT Redox Potentials of Transition-Metal Complexes. *J. Phys. Chem. C* **2012**, *116*, 6349−6356.
(39) Boyer, J. L.; Rochford, J.; Tsai, M.-K.; Muckerman, J. T.; Fujita, E. Ruthenium Complexes with Non-Innocent Ligands: Electron Distribution and Implications for Catalysis. *Coord. Chem. Rev.* **2010**, *254*, 309−330.
(40) Muckerman, J. T.; Fujita, E. Theoretical Studies of the Mechanism of Catalytic Hydrogen Production by a Cobaloxime. *Chem. Commun.* **2011**, *47*, 12456−12458.
(41) Gouterman, M.; Wagnière, G. H.; Snyder, L. C. Spectra of Porphyrins. *J. Mol. Spectrosc.* **1963**, *11*, 108−127.
(42) Lindsey, J. S. *De Novo* Synthesis of Gem-Dialkyl Chlorophyll Analogues for Probing and Emulating our Green World. *Chem. Rev.* **2015**, *115*, 6534−6620.

DOI: 10.1021/acscatal.8b02991
ACS Catal. 2018, 8, 10131−10136